REPORT NO. 118

September, 1958.

THE COLLEGE OF AERONAUTICS

CRANFIELD

An experimental investigation of the subsonic drag and pitching moment characteristics of slender cambered bodies with pointed noses and tails

- by -

K. D. Harris, B.Sc., D.C.Ae.

SUMMARY

It is known that supersonic aircraft are liable to posses some trim drag under cruise conditions. Fuselage camber has been suggested as one means of reducing this component of the drag, and the purpose of this investigation was to obtain quantitative data on the pitching moment increments obtainable from fuselage camber and incidence, and the associated increments in fuselage drag.

Lift, drag and moment measurements have been made on a body representative of the fuselage of a supersonic transport aeroplane. The fineness ratio of the body was 15:1, the cross-sectional area distribution being of modified Sears-Haack form. Parabolic nose and tail camber was used, the nose and tail portions being made removable so that a variety of different configurations could be tested. The Reynolds number of the tests was 14.1×10^6 based on the length of the model, and the Mach number was 0.2. The tests were made with a transition wire attached to the model at 10% of the length from the nose. A preliminary investigation indicated that the Reynolds number was probably sufficiently large to ensure that the results would give a good guide to the full scale characteristics.

The experiments showed that nose camber produces a pitching moment increment in very close agreement with the predictions of inviscid slender body theory. The increments in lift and drag, whilst not zero as predicted by inviscid theory, are small. Tail camber on the other hand gives rise to much larger lift and drag increments, and the increment in pitching moment is quite different from that predicted by inviscid theory. In the present tests the pitching moment increment due to tail camber amounted to about 10% of the theoretical value.

The scope of the experiment was insufficient to answer the question "What is the optimum fuselage shape for minimum trim drag?" However, the indications are that an uncambered fuselage at incidence will provide a given pitching moment for less drag than any cambered fuselage. This however neglects the interference effects of the wing and tail unit on the fuselage, and of the fuselage on the wing and tail unit. For reasons of (i) tail clearance on take-off and landing, (ii) cockpit layout and view, and (iii) cabin layout, fuselages with camber may be required. Some indication of the fuselage drag penalties likely to be sustained by these modifications of the fuselage are given by the results of this experiment.

CONTENTS

Contents Continued

Figures

NOTATION

b	breadth of working section of wind tunnel
C_D	drag coefficient of fuselage based on the maximum cross-sectional area S
C_{D_w}	drag coefficient of fuselage based on the wetted area S_w
$C_{D_{rig}}$	drag coefficient of the rig tail wires based on the area S
C_m	pitching moment coefficient of the fuselage based on the area S and the fuselage length 2 l
$C_{m_{rig}}$	pitching moment coefficient of the rig tail wires based on the area S and length 2 l
D	drag
h	height of working section of wind tunnel
k	calibration factor of wind tunnel
l	semi-length of model
l_1	length of nose and tail portions of model
l_2	length of central portion of model
L	lift
L_m	length of model
M	pitching moment
r	radius of model
R	maximum radius of model
R_N	Reynolds number
S	maximum cross-sectional area of model
S_f	cross sectional area of model
S_w	wetted (or surface) area of model
U	wind speed
U_F	effective free stream speed in working section with model present
U_W	wind speed in working section as determined from a calibration with the working section empty
V	volume of model
x	longitudinal axis with origin at centre of model (see Fig.1)

NOTATION Continued

x_1	longitudinal axis with origin at the base of the nose (or tail) portion of the fuselage (see Fig. 1)
y	axis perpendicular to x-axis (see Fig. 1)
y_c	camber line ordinate
α	local incidence of camber line
$\bar{\alpha}$	incidence of fuselage datum line
γ_n	camber of nose portion, positive when incidence due to camber is positive (see Fig. 1)
γ_t	camber of tail portion, positive when incidence due to camber is positive (see Fig. 1)
ϵ_s	solid blockage factor
ϵ_w	wake blockage factor
μ	coefficient of viscosity of air
ν	kinematic coefficient of viscosity of air
ρ	air density

1. Introduction

It is well known that supersonic aircraft are liable to possess some trim drag (1,2,3) under cruise conditions. In Ref.3 it was suggested that fuselage camber might be used to reduce the magnitude of this trim drag.* Slender body theory was used to determine the amounts of fuselage camber or incidence that might be required by certain typical M = 1.2 project aircraft in order to obtain all the required trimming moment from the fuselage. It was found that large amounts of camber or incidence would probably be required, and it was pointed out that owing to viscous effects the theoretical moments would not be attained in practice. Also, contrary to inviscid theory, it was anticipated that there would be some increase in fuselage drag due to camber or incidence. A programme of wind tunnel tests was therefore proposed to investigate these factors and this report deals with that investigation.

As explained in Ref. 3 the decision to make a series of subsonic tests (in addition to supersonic tests to be made at some other establishment) was governed by the fact that :-

(i) According to slender body theory the pitching moment coefficient of a slender body is independent of Mach number.

(ii) It was desired to test models with pointed tails. This can easily be managed with subsonic models but is not easily accomplished with supersonic models.

(iii) The favilities available at the College at the time of making these tests were far more suitable for subsonic than supersonic testing in view of the high Reynolds number required and the high degree of accuracy demanded in the measurement of the drag and pitching moment.

With item (iii) in mind it was decided that the tests should be made in the College of Aeronautics 8' x 6' tunnel using the largest practicable model. A model length of 10 feet was chosen, and a fineness ratio of 15:1. The length was limited to 10 feet as any greater length would have involved the nose of the model being dangerously near the commencement of the working section (see Fig. 4). With this model in the 8' x 6' tunnel, significant tunnel interference effects might be expected at moderate to large incidences since the nose and tail would touch the floor and roof at about 30° of incidence. However, since the main interest in these tests was for incidences less than about 5° it was decided that a 10 feet long model would be acceptable. The evidence from the tests seems to be that with this model and a wind speed of about 220 feet per second a satisfactorily

---

* This suggestion was first made to the author by Dr. Kuchemann and Mr. Warren of the R.A.E. Farnborough.

large value of the Reynolds number (14.1×10^6) was obtained, giving comparative data which can fairly confidently be used to assess the full scale characteristics of fuselage camber and incidence.

By using a large model a satisfactory level of accuracy was also obtained from the balance readings, although, owing to what is thought to be a temperature effect, it was necessary to adopt the tedious procedure of stopping the tunnel after each wind on reading to take the corresponding wind off reading.

The model used in these tests consisted of a common central portion of circular cross-section and constant diameter. Nose and tail pieces of Sears-Haack area distribution with cambers γ of 0, 0.075 and 0.15 radians were provided. These nose and tail pieces were manufactured so that they could be rotated through 180° thereby permitting a wide range of configurations to be made up, and permitting tests to be made with the models inverted so that corrections could be made for the interference effects of the supporting rig.

The maximum camber of $\gamma = 0.15$ radians was chosen on the grounds that the fuselage surface should nowhere be significantly concave. This amount of camber is less than one half the amount theoretically required (3) for some of the projects (see above), but such large cambers would be quite impracticable from fuselage layout considerations quite apart from aerodynamic considerations.

2. Description of apparatus

2.1. Wind tunnel

All the tests were made in the College of Aeronautics 8' x 6' General Purpose Wind Tunnel. This is a closed working section, return flow tunnel with a contraction ratio of 7:1 and a top speed of about 250 feet per second. At a wind speed of 200 feet per second the turbulent intensity is less than 0.1%. This implies that the results when corrected for tunnel interference effects should be comparable with the results that would be obtained in free flight at the same value of the Reynolds number.

The wind speed is measured using a Betz manometer connected to static pressure tappings situated at the upstream and downstream ends of the contraction. Owing to voltage fluctuations in the power supply the wind speed cannot be maintained constant. At a Betz reading of 250 m.m. of water variations as large as $\pm$ 2 m.m. of water may occur over the course of a few seconds under adverse conditions. Apart from these fluctuations which occur at irregular intervals the speed remains constant to within about $\pm$ 0.2 m.m. of water as measured on the Betz manometer.

2.2. Balance

The balance is a Warden type six component balance as manufactured by Test Equipment Ltd.

The sensitivity of this balance is such that the lift indicator can easily be balanced out to within ± 0.01 of a revolution, whilst the drag and pitching moment indicators can be balanced out to within the same values provided great care is taken. One revolution of each indicator corresponds to five revolutions of the appropriate lead screw and the sensitivities correspond approximately to ± 0.05 lb. of lift, ± 0.004 lb. of drag and ± 0.03 lb. ft. of pitching moment.

During the course of this experiment it was found that the wind off zero readings of the drag and pitching moment balances changed significantly over the course of an hour of running the tunnel. The steps taken to overcome this difficulty are described in paragraph 3.

2.3. The model

The model, see Fig. 1, which was made of laminated mahogany, consisted of an uncambered central portion of length 3 feet with a circular cross-section of 8 inches constant diameter. The detachable nose and tail portions were of Sears-Haack area distribution, and the camber lines were parabolic in shape (see Appendix I). Three nose and tail portions were manufactured having cambers of 0, 0.075 and 0.15 radians. The radius and camber distributions are given in Table I. (The camber is defined to be positive when the camber line slope is nose up relative to the fuselage datum line). Each nose and tail was manufactured so that it could be rotated through 180°. Owing to slight errors in manufacture and uneven shrinking of the timber small steps amounting to less than 0.01 inches were present between the nose and tail and central portions. These steps were partially faired by means of strips of Sellotape wound round the model.

The model was supported (Fig. 2) from a single strut. The model was pivoted about its centre, which coincided with the virtual centre of the balance. The strut was shielded by a streamline fairing cut away at its lower end to permit the model to be rotated through an incidence range from -12° to +15°.

The incidence was controlled by V wires wound on a motor operated winch attached to the balance turntable. A selsyn type counter was used to record the revolutions of the winch.

2.4. Transition wire

The main series of tests was made with a 0.014 inch diameter transition wire fixed 12 inches aft of the nose of the model. For the Series I tests

these wires were attached by means of four 1 inch wide strips of Sellotape. For the Series II tests the wires were glued into very fine grooves scribed around the nose.

2.5. Turbulence grid

A few tests were made with a turbulence grid upstream of the model. This grid, which is shown in Fig. 3 consisted of twelve 5/16" diameter ropes running from the floor to the roof of the working section, the pitch being 2". This grid was mounted approximately 26" upstream of the nose of the model. The tunnel speed for this test was measured with a single pitot-static tube (see Fig. 3). These calibrations were made with the model in the working section, and must be considered rather approximate.

3. Details of Test

3.1. Tail wire contribution to pitching moment

The contribution of the V wires to the pitching moment can be estimated (see Appendix III) but the contribution of the counterweight tail wire depends on the moment which can be transmitted through the attachment of this wire to the model. Since this is not amenable to calculation a test was made to determine the magnitude of this term. A drag load equal to the estimated drag of the wire was applied at a point midway between the attachment to the model and the floor of the tunnel. The pitching moment due to this drag load was measured on the balance, and from this reading the effective moment arm of the tail wire drag could be calculated. This was done over the full incidence range of the model.

3.2. Incidence calibration

An incidence calibration was made for each configuration prior to the commencement of the wind on tests. The incidence was measured by a sensitive inclinometer placed on the rear end of the centre portion of the model. Checks made during the course of the experiment showed that the incidence setting obtained using this calibration was better than $\pm$ 0.1, wind off. Incidence measurements were not made with the wind on but owing to the relatively small pitching moment produced by the model the errors due to this effect were found to be negligible. The incidence, unless otherwise stated, has been taken as positive with the nose down in the tunnel (i.e. the convention used for an inverted model).

3.3. Initial tests

Prior to embarking on the main series of tests it was decided to make some initial tests to determine the influence of variation of Reynolds number and various forms of forced boundary layer transition. Details of these tests are tabulated below :-

(i) Body of revolution, $\tilde{\alpha} = 0^{\circ}$

The drag coefficient was measured with :-

(a) free transition, and
(b) a 0.014" diameter transition wire taped round the body 12" aft of the nose, for the following values of wind speed and Reynolds number :-

U_T (f.p.s.)	$R \times 10^{-6}$
98.6	6.30
139.5	8.92
170.9	10.93
197.3	12.6
220.8	14.1

(ii) Cambered body ($\gamma_n = -0.15$, $\gamma_t = -0.15$)

C_L, C_D and C_m were measured over the incidence range from -12° to $+12^{\circ}$ for the following configurations :-

Model Configuration	U_T f.p.s.	$R \times 10^{-6}$
Free transition	98.6 220.8	6.30 14.1
0.014" diameter transition wire taped around the body 12" aft of the nose	98.6 220.8	6.30 14.1
Turbulence grid 26" upstream of the nose of the model	91.7 20.5	5.86 13.1

3.4. Main tests - Series I

From the initial tests it was concluded (see paragraph 5.1) that the most satisfactory comparative results would be obtained using a transition wire and the highest practicable wind speed of 220.8 f.p.s. ($R_N = 14.1 \times 10^6$).

Owing to the interference effects of the strut, strut fairing and tail wires it was decided that each configuration should be tested through both the positive and negative incidence ranges with the model the 'right way up' and 'inverted' (i.e. the nose and tail portions rotated through 180° about the body axis). Approximate allowance could then be made for the interference effects of the rig by taking the arithmetic mean of the two sets of results.

For these tests the transition wire was attached to the model by means of four pieces of inch wide Sellotape, the pieces of Sellotape being placed at 0°, 90°, 180° and 270° to the vertical plane of symmetry through the model. The wind on readings were taken through the full incidence range from -12° to $+12^\circ$, followed by the wind off zero readings.

3.5. Main tests - Series II

Analysis of the above series of tests suggested that the drag measurements were not entirely consistent. Two explanations for this appeared likely. Firstly, it was observed that the method of fixing the transition wires did not ensure that there were no gaps between the wire and the model. Any variation in gap between one model configuration and another would lead to variations in drag owing to the different drags of the wire themselves. Secondly, observation of the measured data showed that the wind off zero readings of the drag balance which should have been the same throughout the whole series of tests actually showed some variation. A second series of tests was therefore made to try to eliminate these causes of error.

The errors caused by the variation of transition wire drag were reduced as much as possible by glueing the wires into very fine grooves scribed round the bodies.

The drift of the wind off zero reading was investigated by taking a series of wind on and wind off readings. This investigation showed that provided each wind on measurement was immediately followed by the corresponding wind off measurement the drag coefficient was repeatable to within $\pm$ 0.0005 at a wind speed of 220.8 f.p.s. This is in close agreement with the estimated value of $\pm$ 0.0004 based on the assumption that the drag can be measured to the nearest $\pm$ 0.01 of a revolution wind on and wind off (see Appendix IV).

From this investigation it was concluded that an acceptable level of accuracy could be obtained provided each wind on reading was immediately

followed by the corresponding wind off reading. Because of the very considerable increase in time involved in following this procedure it was decided to restrict the range of investigation to -4° to $+4^{\circ}$ of incidence. After about two hours of running the zero readings usually became nearly constant. When this occurred a zero reading was taken prior to the commencement of the wind on tests, and a check reading was taken after the completion of these tests. Where any slight change of the zero reading was observed the zero readings were varied linearly with time.

It seems probable that the drift of the zero readings is due to a temperature effect. Attempts to reduce or eliminate the drift by leaving heaters in the balance chamber on all night were however unsuccessful.

3.6. Surface flow visualisation

An attempt was made to study the surface flow using a mixture of alabastine in teepol. This proved unsuccessful owing to gravitational effects and the relatively small value of the skin friction over the rear of the model. However, observation of the flow of the mixture whilst it was still wet confirmed that there was a flow separation over the leeward side of the tail. This was also confirmed by tracking a nylon tuft towards the surface of the body. On approaching the body the flow direction could be seen to change fairly abruptly indicating the existence of a vortex of the type associated with flow separation from a body.

At all times the tuft, which was about one inch in length, remained steady and did not gyrate rapidly as it has been observed to do when placed in the vortices formed by swept back and delta wings.

4. Results

4.1. Corrections to observed results

4.1.1. Rig drag

The estimated drag of the tail wires has been subtracted from the observed data (see Appendix III).

The direct drag of the strut and the interference drags of the strut, the strut fairing and the tail wires have been neglected. The direct drag of the strut is certainly not negligible but it is not amenable to calculation and since the main purpose of the tests was to determine the drag increments due to incidence and camber it was decided to neglect this correction.

From Fig. 5 it will be seen that the drag of the tail wires is approximately equal to the zero incidence drag of the body of revolution. Any error in estimating the drag of the wires will therefore have about the same percentage error on the quoted drags of the bodies.

4.1.2. Rig pitching moment

The estimated pitching moment of the V wires and the 'part estimated - part measured' pitching moment of the counterweight tail wire have been subtracted from the measured pitching moment.

4.1.3. Pressure gradient correction to drag

The horizontal buoyancy due to variation of the static pressure coefficient in the working section (Fig. 4) has been calculated, - see Appendix III. To correct for this effect the observed drag coefficient results should be increased by 0.0013, or rather less than 1% of the minimum drag coefficient of the body of revolution.

This correction has been neglected.

4.1.4. Blockage

In Appendix III it is shown that due to solid plus wake blockage the effective free stream velocity U_F is equal to about 1.006 times the tunnel velocity U_T. To correct for this effect the observed coefficients (including rig drag) should be decreased by about 1%. Allowing for the drag of the rig the quoted values of body drag should be decreased by about 2%.

This correction has been neglected. Combined with the blockage correction the quoted drag coefficients should therefore be decreased by about 1%.

4.2. Accuracy of results

Owing to uncertainty about the magnitude of certain corrections the absolute accuracy of the results cannot be stated. Owing to neglect of the pressure gradient and blockage corrections all the quoted results are very approximately 1% high.

The scatter in the results caused by errors in measuring the balance are not known with any accuracy for the Series I tests, but for the Series II tests which have been used in all the quantitative results presented in this section and discussed in paragraph 5 the scatter should not exceed the following (see Appendix IV) :-

Coefficient	Accuracy	
	U = 98.6 f.p.s.	U = 220.8 f.p.s.
C_L	± 0.026	± 0.006
C_D	± 0.002	± 0.0004
C_m	± 0.002	± 0.0004

4.3. Averaging of results

As explained in paragraph 3 tests were made with each model configuration the right way up and inverted. In Figs. 13 to 17 both sets of results have been plotted so that the differences can be seen at a glance. In Figs. 18 to 22 the points plotted are the mean of the two sets of measurements. The reason for the discrepancy between the two sets of measurements has been assumed to be due to the interference effect of the strut and strut fairing and it has been assumed that this interference effect can be eliminated by taking the mean of the two sets of results. Whilst the former assumption is probably valid it should be noted that the latter assumption may not be strictly correct.

4.4. Comparison of experimental results with those of slender body theory

Configuration	γ_n / γ_t	0 / 0	0.075 / 0	0.15 / 0	0 / 0.15	0.15 / 0.15	0.15 / -0.15
$C_{L_{\alpha=0}}$	Theory	0	0	0	0	0	0
	Exp.	0	0.0025	0.005	0.029	0.036	-0.024
$\left(\frac{\partial C_L}{\partial \alpha}\right)_{\alpha=0}$	Theory	0	0	0	0	0	0
	Exp.	0.71	0.78	0.75	0.82	0.82	0.79
$C_{m_{\alpha=0}}$	Theory	0	0.0105	0.021	0.021	0.042	0
	Exp.	0	0.011	0.021	0.002	0.022	0.019
$\left(\frac{\partial C_m}{\partial \alpha}\right)_{\alpha=0}$	Theory	1.42	1.42	1.42	1.42	1.42	1.42
	Exp.	1.04	1.03	1.02	0.98	1.00	0.99

$\left(\frac{\partial C_L}{\partial \alpha}\right)_{\alpha=0}$ and $\left(\frac{\partial C_m}{\partial \alpha}\right)_{\alpha=0}$ have been evaluated over the range from $\bar{\alpha} = -2^\circ$ to $\bar{\alpha} = +2^\circ$

5. Discussion

5.1. Reynolds number and forced transition effects

In Fig. 7 the drag coefficient C_{D_w} (based on wetted area) is plotted against the Reynolds number for the body of revolution at zero incidence with and without a transition wire. For comparison curves of the drag coefficient as estimated from the Royal Aeronautical Society Data Sheets (5) are also included.

Without the transition wire the drag coefficient increases markedly as R_N increases from 6.3 to 10.9 x 10^6, thereafter decreasing very slightly with further increase in R_N up to 14.1 x 10^6. Comparison with the estimated curves suggests that the position of transition moves forward with increase of R_N up to 10.9 x 10^6 and thereafter remains approximately fixed in position. This deduction is further substantiated by the experimental results obtained with the transition wire at 0.1 L_m (although at the lower values of R_N the transition wire was almost certainly insufficiently large to cause immediate transition).

The fact that the experimentally determined drag was higher than that predicted by Ref. 5 is only to be expected since no allowance has been made for the drag of the strut and the interference drags of the strut, the strut fairing and the tail wires. Also, no corrections were made for blockage or tunnel static pressure gradient. The blockage correction would decrease the drags by about 2% (allowing for the wire drag of the rig) whilst the static pressure gradient would increase the drags by about 1%; an overall decrease of about 1%.

Figs. 8 and 9, which are for the case of $\gamma_n = \gamma_t = 0.15$,[X] show the effect of artificially varying the nature of the boundary layer by the use of a transition wire and a turbulence generating grid. At the lower Reynolds number of 6.3[*] x 10^6 (Fig. 9) the lift, drag and pitching moment characteristics are all affected by the changes in the boundary layer condition. At the higher Reynolds number of 14.1[*] x 10^6 (Fig. 8) only the drag results are appreciably affected by these changes in boundary layer conditions.

X In the figures 8 - 12 inclusive the incidence is taken as positive with nose up in the tunnel. The reason for the change in sign convention is that for this series of tests, on the effect of Reynolds number, the bodies tested had negative nose and tail cambers, but for comparison with the remaining tests it is preferable to refer to these as positive nose and tail camber with the consequent changes in sign convention.

* The Reynolds numbers are slightly lower for the tests with the turbulence grid.

A peculiarity of the drag results is a kink in the curves between $\alpha = 0^{\circ}$ and $\alpha = 3^{\circ}$ for the transition free tests. This feature is not present in the results obtained with the transition wire or the turbulence grid. This suggests that the kink is due to free movement of the transition front with change of incidence. At full scale values of the Reynolds number transition would be nearer the nose than in these tests, and the position of the front would vary little with incidence (for the small incidences in which we are interested). It therefore seems reasonable to conclude that better comparative data will be obtained by making the tests on the different body configurations with a transition wire. (The turbulence grid might be used in place of the transition wire but its effect would probably be too severe, and in any case a proper calibration of the working section with the turbulence grid in position is not available).

Figs. 10, 11 and 12 show the effect of change of Reynolds number. With free transition (Fig. 10) the lift and drag characteristics are appreciably affected by change of R_N, whilst the pitching moment characteristics are only slightly affected. With the transition wire (Fig. 11) the lift and drag as well as the pitching moment characteristics are little affected by change of R_N. Fig. 12 shows that the turbulence grid has a similar effect to that of the transition wire in making the characteristics almost independent of change of Reynolds number. There is however one respect in which the results seem to be more influenced by change of R_N with the wire or grid than with free transition and that is in the lift characteristics near zero incidence. However it is shown in Appendix IV that the possible scatter in the lift coefficient results may amount to $\pm$ 0.026 at the lower test Reynolds number. Bearing in mind that these tests were also made using the technique of measuring the balance wind off zero readings after measuring the wind on readings through the full incidence range it is quite conceivable that this apparent Reynolds number effect is spurious.

The general conclusion drawn from these results is that a test Reynolds number of 14.1×10^6 is sufficiently large to give reliable comparative data. In fact, in so far as the lift characteristics are concerned, comparison of Figs. 8 and 9 will show that except for the case of free transition with low Reynolds number almost identical results are obtained at the high and low Reynolds numbers for all three conditions of the boundary layer. The same is true to a somewhat lesser extent with the pitching moment characteristics.

From these tests it was therefore decided to make the main series of tests at a Reynolds number of 14.1×10^6 and to use a transition wire to eliminate the kinks in the drag curves.

5.2. Incidence and camber effects

The results of the Series I tests are given in Figs. 13 to 17. Whilst the drag results of this series of tests are somewhat inaccurate for the reasons outlined in paragraph 3.5 the results of this series serve to show the general nature of the lift, drag and pitching moment characteristics over a wider range of incidence than do the Series II tests.

The first point worthy of note is the good agreement of the lift and pitching moment results with the model the right way up and inverted. This is particularly true of the pitching moment results, and it suggests that taking the arithmetic mean of the two sets of results should yield an accurate correction to the lift and pitching moment results for the interference effects of the strut and its fairing. The agreement between the two sets of drag results is far poorer. Inspection of the graphs shows that the drag is invariably higher when the model is tail down. This seems reasonable since the strut and fairing are then on the leeward side of the model and might be expected to cause a greater interference drag than when on the windward side of the model. In this connection Fig. 23 showing C_D plotted against $C_L \tan \alpha$ is of interest. The nose down (tail up) results give, very nearly, $C_D = 0.178 + C_L \tan \alpha$. Now if the skin friction drag remains constant with change of incidence we would expect the drag coefficient to vary approximately* as $C_L \tan \alpha$. This result suggests that the interference drag due to the strut and its fairing may be almost constant when the nose is down in the tunnel and that a more accurate measure of the drag would be obtained by plotting the curves to pass through the points measured with the nose down. However, since there is insufficient evidence to support this hypothesis the drag curves have in all cases been taken as the mean of the nose up and nose down tests.

The theoretical $C_m \sim \alpha$ relationship as predicted by slender body theory has been evaluated (see Appendix II) and has been plotted in each figure. From Fig. 14 and the table in paragraph 4.4 it will be seen that at $\bar{\alpha} = 0^\circ$ the cambered nose plus uncambered tail configuration produces almost exactly the theoretical pitching moment coefficient. Moreover the lift coefficient is at the same time very close to the theoretical value of zero. This shows that the flow over the nose of such a cambered body approximates very closely to the theoretical inviscid flow except for the presence of a thin boundary layer. From Fig. 15 and the table in paragraph 4.4 it will be seen that the same is not true of the body with cambered tail and uncambered nose. In this case the pitching moment coefficient produced by the tail at $\bar{\alpha} = 0^\circ$ is only about 10% of the

---

* C_D would only vary as $C_L \tan \alpha$ if the positive increment in pressure on the lower half of the body was accompanied by an equal negative increment on the upper half. Since the lift is primarily caused by separation of the flow and the formation of body vortices it follows that C_D will only vary approximately as $C_L \tan \alpha$.

theoretical value and the lift coefficient is not zero. It is evident as confirmed by the tuft tests (paragraph 3.6) that flow separation is occurring on the leeward side giving rise to the well known type of vortex flow associated with bodies at incidence.

In Fig. 13, which is for the body of revolution, the theoretical $C_m \sim \alpha$ relationship is plotted for the nose alone and for the nose plus tail. The theoretical $C_L \sim \alpha$ relationship for the nose alone is also plotted. Since the results referred to above indicate that the cambered nose must have flow characteristics very similar to the characteristics predicted by inviscid theory it seems likely that the nose of the body of revolution would also have characteristics very similar to those predicted by theory over a small incidence range - say $\pm 2^\circ$. If this is accepted it becomes apparent that the uncambered tail is only providing about 40% of the theoretical positive pitching moment and about 60% of the theoretical negative lift which it should produce at incidence (over the range of $\pm 2^\circ$).

The results of the Series II tests are shown in Figs. 18 to 22 where only the mean results are plotted. The lift and moment results are in close agreement with those of the Series I tests, but except for the 'banana fuselage' ($\gamma_n = 0.15$, $\gamma_t = -0.15$) the drag coefficients are slightly lower for the Series II tests. Lower drags would be expected in the Series II tests owing to the fact that in the Series I tests the transition wires stood slightly proud of the surface at some points around the periphery.

The results given in the table in paragraph 4.4, which have already been referred to above, have been based on the Series II tests.

5.3. Comparison of the various configurations

The primary object of this experiment was to obtain quantitative data on the drag and pitching moments due to incidence and camber. To facilitate comparison of the results the mean drag coefficients from the Series II tests have been plotted against incidence in Fig. 18 and against the mean pitching moment coefficient in Fig. 19. Fig. 20 is also a plot of $C_D \sim C_m$, but to assist in comparing the drags the drag scale has been considerably enlarged and the results have been presented in such a way that the results from all the possible camber configurations can readily be compared. The possible range of scatter of the drag points is shown on this figure. The scatter is sufficiently small to permit confidence to be placed in the comparison of the results.

Referring first to Fig. 18 it will be seen that at zero incidence the drag is least for the body of revolution. Replacing the uncambered nose by the $\gamma = 0.15$ nose results in a small increase in drag. The increase in drag caused by replacing the tail of the body of revolution by the $\gamma = 0.15$ tail is much larger. It is interesting to note that the drag

with the cambered tail is almost independent of the nose camber.

With change of incidence from zero the drag increment due to camber varies in the expected manner; that is to say the drag increment increases when the combined incidence due to datum line incidence plus fuselage camber line incidence increases numerically and decreases when the combined incidence decreases numerically.

The object of using fuselage incidence or camber is to produce a positive contribution to the pitching moment coefficient to assist in trimming the aircraft under cruise conditions. From Fig. 20 it appears that for the particular range of configurations chosen for these tests the minimum drag will be obtained by using a body of revolution at incidence for any value of C_m up to about 0.07. For higher values of C_m a lower drag is given by an uncambered nose and a swept up tail (negative γ), but since the datum line incidence would then exceed 4° and the fuselage drag increment relative to the minimum fuselage drag would exceed 4% it seems unlikely that a C_m in excess of 0.07 would be used in practice. However, the upswept tail configuration might still be required in preference to a completely uncambered fuselage owing to the greater tail clearance that would be available for take-off and landing.

From the drag point of view the fuselage with postively cambered nose and zero tail camber is nearly as good as the uncambered fuselage, and it has the advantage of producing a given pitching moment for a smaller datum line incidence.

The other configurations which might possibly be of some use are the negatively cambered nose and tail fuselage and the 'banana' fuselage with positive nose camber and negative tail camber. The former however requires a larger datum line camber than any of the other configurations to produce a given C_m. Both configurations will lead to at least a 3% to 4% increase in fuselage drag as compared with the body of revolution at zero incidence.

Figs. 21 and 22 are plots of $C_m \sim \alpha$ and $C_L \sim \alpha$ to large scales. Fig. 21 shows the very small C_m increment contributed by the cambered tail. Fig. 22 shows the much larger C_L increment that is produced by tail camber as against nose camber and also shows that the effects of nose camber and tail camber measured separately can be combined to determine the effects of combined nose and tail camber.

The tests referred to so far in this discussion have been confined to various configurations with nose and tail cambers of 0.15. The Series II tests included one test with a nose camber of 0.075 and zero tail camber. The mean results from this test are shown in Fig. 24 where the results for $\gamma_n = 0$ and 0.15 are also shown. It will be seen that whereas the C_m results

vary linearly with nose camber, as would be expected from the close agreement of experiment with theory, the C_D results do not vary linearly with camber. The drag results are not easy to explain since it would appear that at zero incidence the drag increment due to 0.075 nose camber is as great as the increment due to twice this amount of camber. Possibly this is a case in which the possible range of scatter of the results combined with small errors in manufacture of the models have combined to produce a misleading result.

5.4. Limitations of the experiment

It must be emphasised in concluding this discussion that this experiment has a number of limitations in so far as applying it to estimate the drag of a complete supersonic aircraft is concerned. The main limitations would seem to be :-

(i) the relatively low value of the Reynolds number,

(ii) the low Mach number ($M = 0.2$),

(iii) the absence of interference effects on the fuselage due to a lifting wing and, to a lesser extent, the tail unit,

(iv) the influence of the flow perturbations due to fuselage incidence and camber on the performance of the wing and tail unit.

There is some evidence from these tests that the effect of item (i) may be small. The effect of the low Mach number of these tests may well be important, but this effect can only be determined by a comparable series of tests at higher Mach numbers at other establishments. The interference effects listed under items (iii) and (iv) might also be expected to be important. The body vortices due to incidence or camber might have a considerable effect on the performance of the tailplane; particularly the spanwise distribution of lift.

6. Conclusions

This experiment has shown that nose camber gives a pitching moment increment very close to that predicted by inviscid slender body theory. The drag penalty, which is zero on inviscid theory, is quite small, and so is the increment in fuselage lift. On the other hand tail camber does not give results agreeing with inviscid theory. The drag and lift increments are several times larger than those due to nose camber, and the pitching moment increment is quite unrelated to the theoretical increment. For the model tested in this experiment the pitching moment increment due to tail camber, measured about the mid point of the model, was about 10% of the theoretical moment increment.

The optimum fuselage configuration for minimum trim drag of a supersonic aircraft cannot be deduced from this investigation owing to the

fact that interference effects from the fuselage on the flow over the wings and tail unit, and from the wings and tail unit on the fuselage, have not been studied; nor was the test made at supersonic speed. However, the evidence seems to be that for a given increment in pitching moment the minimum fuselage drag is given by an uncambered body at incidence. Practical considerations of obtaining adequate ground clearance of the tail for take-off and landing may demand the use of negative tail camber. The experiment shows that such camber can be used with little, if any, adverse effect on the pitching moment of the fuselage for a given datum line incidence. The drag penalty of such negative tail camber may be considerable at zero incidence, but as fuselage incidence increases the drag penalty decreases until above a certain value of incidence or pitching moment the drag is actually decreased by negative tail camber. In the present experiment with $\gamma_t = -0.15$ radians this occurred at about 4° (0.07 radians) of incidence.

The other configurations which might possibly be of some use, both of them having negative tail camber, are the configurations with either positive or negative nose camber. The former gives a reduction in fuselage incidence for a given pitching moment whilst the latter requires a larger incidence than the other configurations to develop a given pitching moment but it gives a more favourable nose shape for the layout and view from the cockpit. Both configurations lead to significant increases of fuselage drag - about 3% to 4% for the models tested.

7. Acknowledgements

The author is indebted to Mr. G.G.Appleby and Mr. R. Malet de Carteret for their help in conducting the experiment and reducing the results. Also Mr. C.D.Bruce and Mr. L. Wilsher who painstakingly made the models and Mr. S. Lilley who helped with a number of small yet important practical items.

8. References

1. Richardson, J.R. — Notes on drag-due-to-lift and trim drag. (Unpublished). 1957.

2. Harris, K.D. — Comments on 'Trim Drag'. (Unpublished). 1957.

3. Harris, K.D. — The use of fuselage camber and incidence as a means of reducing the trim drag of supersonic aircraft. (Unpublished) 1957.

4. Pankhurst, R.C. Holder, D.W. — Wind-tunnel technique. Pitman.

5. - — The Royal Aeronautical Society Data Sheets, Volume I, Bodies 02.04.01 and .02.

APPENDIX I

Model Data

1. Area and camber distributions

The central portion, common to all the models, is uncambered, 3 feet in length with a circular cross-section 8 inches in diameter.

The nose and tail portions are of circular cross-section with a Sears-Haack area distribution, namely :-

$$S_f = \frac{\pi R^2}{l_1^3} \left\{ l_1^2 - x_1^2 \right\}^{3/2}$$

where $R = 4"$

$l_1 = 42"$

The camber lines are parabolic in form, i.e.

$$\frac{dy_c}{dx_1} = \gamma \frac{x_1}{l_1}$$

or $$y_c = \frac{\gamma}{2l_1} x_1^2$$

Three sets of nose and tail portions were made with cambers

$$\gamma = 0,\ 0.075 \text{ and } 0.15 \text{ radians.}$$

The actual radius and camber distributions are given in Table I.

2. Reference areas

Maximum cross-sectional area S

$$S = 0.349 \text{ sq.ft.}$$

Surface (or wetted area) S_W

For the purpose of comparing the drag results with estimated data the drag coefficient C_{D_W} was based on the wetted area S_W

$$S_W = 16.81 \text{ sq.ft.}$$

3. Volume V

$$V = 2.484 \text{ cu.ft.}$$

APPENDIX II

Theoretical estimates of the lift and pitching moment characteristics

1. Slender body theory

According to slender body theory the lift intensity per unit length on a body of circular cross-section is :-

$$\frac{dL}{dx} = \rho U^2 \frac{d}{dx} (S_f \alpha) \tag{1}$$

$$\therefore \quad L = \rho U^2 \left[S_f \alpha \right]_{-l}^{l} \tag{2}$$

The pitching moment is

$$M = - \rho U^2 \int_{-l}^{l} \frac{d}{dx} (S_f \alpha) \, x \, dx \tag{3}$$

Integrating by parts

$$M = - \rho U^2 \left\{ \left[x S_f \alpha \right]_{-l}^{l} - \int_{-l}^{l} S_f \alpha \, dx \right\} \tag{4}$$

2. Theoretical estimates

2.1. Overall lift

From (2), since all the models are pointed at the tail (and nose), the overall lift is zero independent of camber or incidence.

2.2. Pitching moment due to camber

From Ref.3 the pitching moment due to positive nose and tail camber at zero incidence ($\bar{\alpha} = 0$) is

$$M = \rho U^2 \gamma \pi R^2 \frac{2}{5} l_1$$

i.e. $$\boxed{C_m = \frac{2}{5} \gamma \frac{l_1}{l}}$$

APPENDIX II Continued

2.3. Pitching moment due to incidence

Consider the uncambered body at incidence $\bar{\alpha}$. The nose portion will carry a lift L_n, the central portion will carry no lift, and the tail portion will carry a lift L_t which will be equal in magnitude but opposite in sign to that of the nose lift L_n. The pitching moment due to incidence may therefore be obtained by estimating L_n (and L_t) and the centre of pressure position of the nose (and tail).

From (2)

$$L_n = \rho U^2 S \bar{\alpha}$$

From (4) the moment M_n about the rear of the nose portion is

$$M_n = \rho U^2 \int_{-l_1}^{0} S_f \bar{\alpha} \, dx_1$$

$$= \rho U^2 \bar{\alpha} \int_{-l_1}^{0} S_f \, dx_1$$

The latter integral is the volume of the nose.

$$\int_{-l_1}^{0} S_f \, dx_1 = \int_{-l_1}^{0} \frac{\pi R^2}{l_1^3} (l_1^2 - x_1^2)^{3/2} \, dx_1$$

$$= \frac{3}{16} \pi^2 R^2 l_1$$

Hence $M_n = \rho U^2 \bar{\alpha} \frac{3}{16} \pi S l_1$

Thus the centre of pressure of the nose is at

$$x_{1_{c.p.}} = \frac{M_n}{L_n} = \frac{3}{16} \pi l_1$$

The total pitching moment on the body at incidence is therefore

$$M = 2 \rho U^2 S \bar{\alpha} \left\{ \frac{3}{16} \pi l_1 + \frac{l_2}{2} \right\}$$

$$\therefore \quad \boxed{C_m = \frac{2\bar{\alpha}}{l} \left\{ \frac{3}{16} \pi l_1 + \frac{l_2}{2} \right\}}$$

i.e. $C_m = 1.424 \bar{\alpha}$

or $\frac{dC_m}{d\alpha} = 1.424$

APPENDIX III

Reduction of Results

1. Dynamic pressure and velocity

From the tunnel calibration dated 19.8.55

$$k = 1.13$$

where

$$k = \frac{\frac{1}{2}\rho U_w^2}{(p_s - p_w)_B}$$

Now $$(p_s - p_w)_B = \frac{5.202}{25.4} h \text{ lb./sq.ft.}$$

where h is the Betz reading in m.m. of water.

Hence $$\frac{1}{2}\rho U_w^2 = 1.13 \times \frac{5.202}{25.4} \times h$$

i.e. $$\frac{1}{2}\rho U_w^2 = 0.2315\ h \text{ lb./sq.ft.}$$

and $$U_w = 13.95 \sqrt{h} \text{ f.p.s.}$$

2. Balance calibration

The balance calibrations given by preliminary tests (which did not include the effects of interference) are :-

$$L = 5.155 (R_1 - R_{1_z}) \quad \text{(lb.)}$$

$$D = 0.423 (R_4 - R_{4_z}) \quad \text{(lb.)}$$

$$M = -3.068 (R_{4_a} - R_{4_{a_z}}) \quad \text{(lb.ft.)}$$

3. Evaluation of coefficients(uncorrected)

$$C'_L = \frac{L}{\frac{1}{2}\rho U^2 S} = 63.8 \frac{R_1 - R_{1_z}}{h}$$

$$C'_D = \frac{D}{\frac{1}{2}\rho U^2 S} = 5.23 \frac{R_4 - R_{4_z}}{h}$$

$$C'_{D_w} = \frac{D}{\frac{1}{2}\rho U^2 S_w} = 0.1087 \frac{R_4 - R_{4_z}}{h}$$

$$C'_m = \frac{M}{\rho U^2 S l} = -3.795 \frac{R_{4_a} - R_{4_{a_z}}}{h}$$

APPENDIX III Continued

4. Tunnel interference corrections

4.1. Static pressure gradient

Because of the length of the model the static pressure gradient cannot be treated as a constant, and so the standard methods of estimating the correction to the drag coefficient are inapplicable. To obtain an approximate guide to the magnitude of this correction we may calculate the horizontal buoyancy.

The drag coefficient due to the horizontal buoyancy is

$$\Delta C_{D_S} = \frac{1}{\pi h^2} \int_{-l}^{l} C_{p_s} \; 2\pi r \; dr$$

where

C_{p_s} = static pressure coefficient along centre line of empty working section.

C_{D_S} has been evaluated by graphical integrations giving

$$\Delta C_{D_S} = -0.0013$$

This amounts to slightly under 1% of the minimum drag coefficient of the body of revolution.

4.2. Blockage corrections

$$U_F = U_T \; (1 + \epsilon_s + \epsilon_w)$$

where ϵ_s = solid blockage factor

and ϵ_w = wake blockage factor

The solid blockage factor ϵ_s is approximately given (Ref. 4, p.344) by

$$\epsilon_s = 0.65 \; \frac{V}{h^2 b}$$

where V = volume of body plus fairing
h = height of working section
b = breadth of working section

APPENDIX III Continued

The wake blockage factor is given (Ref. 4, p.348) by

$$\epsilon_w = \frac{1}{4} \frac{S}{bh} C_D$$

where S is the area on which C_D is based, and C_D is the overall drag coefficient including the fairing. Substituting in these two formulae we have

$$\epsilon_s = 0.0056$$
$$\epsilon_w = 0.00031$$

Hence, $U_F = 1.0058\ U_T$

Thus the effective free stream velocity U_F is a little more than ½% greater than the tunnel velocity U_T.

4.3. Rig correction

Rig drag coefficient $C_{D_{rig}}$

The drag of the tail wires has been calculated assuming a drag coefficient of unity based on frontal area. The rig drag coefficient $C_{D_{rig}}$ based on the model reference area S of the model is plotted in Fig. 5.

It will be seen that the wire drag is approximately equal to the zero incidence drag of the body of revolution.

Rig pitching moment coefficient $C_{m_{rig}}$

To determine the contribution of the counterweight tail wire to the pitching moment a drag load was applied to the wire midway between its attachment to the fuselage and the floor. The pitching moment was read on the balance and hence the effective moment arm of the drag load was found. This effective moment arm is plotted in Fig. 6(a).

Using the estimated tail wire drags referred to above the pitching moment due to the tail wires was then calculated. The wire pitching moment coefficient $C_{m_{rig}}$ based on the model reference area S and reference length 2 l is plotted in Fig. 6(b).

APPENDIX IV

Accuracy of the results

The sensitivity of the balance is such that the revolution counters can be balanced out to within the following limits :-

Lift balance	± 0.01
Drag balance	± 0.01
Pitching moment balance	± 0.01

These limits apply with wind on and wind off and lead to the following limits in the determination of the coefficient.

Coefficient	Accuracy	
	U = 98.6 f.p.s.	U = 220.8 f.p.s.
C_L	± 0.026	± 0.006
C_D	± 0.002	± 0.0004
C_m	± 0.002	± 0.0004

The Betz manometer could be read to the nearest 0.1 m.m. of water but owing to the unsteadiness of the tunnel velocity it would probably be more realistic to assume that the accuracy of measurement was to within ± 0.2 m.m. of water. This corresponds to an accuracy of ± 0.2% in the measurement of the speed at 98.6 f.p.s. and ± 0.04% at 220.8 f.p.s.

TABIE I

Radius and camber line distributions

x_1 (ins.)	y_c (ins.)		r (ins.)
	= 0.075	= 0.15	
0	0	0	4.000
8.4	0.063	0.126	3.879
16.8	0.252	0.504	3.510
21.0	0.394	0.788	3.224
25.2	0.567	1.134	2.862
29.4	0.772	1.544	2.414
33.6	1.008	2.016	1.859
37.8	1.276	2.552	1.107
39.9			0.698
42.0	1.575	3.150	0

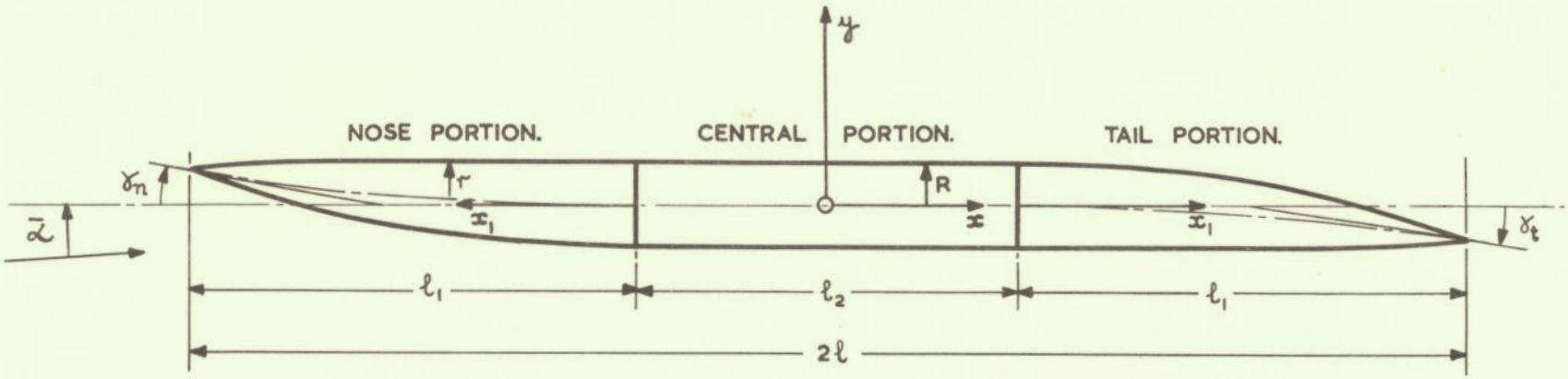

$R = 4''$ FOR RADIUS r & CHAMBER LINE DISTRIBUTIONS.
$\ell_1 = 3{\cdot}5'$ SEE TABLE I.
$\ell_2 = 3'$ γ_n & γ_t ARE POSITIVE AS SHOWN.

SCALE:— 1/12 FULL SCALE.

FIG. I. DIAGRAM OF MODEL.

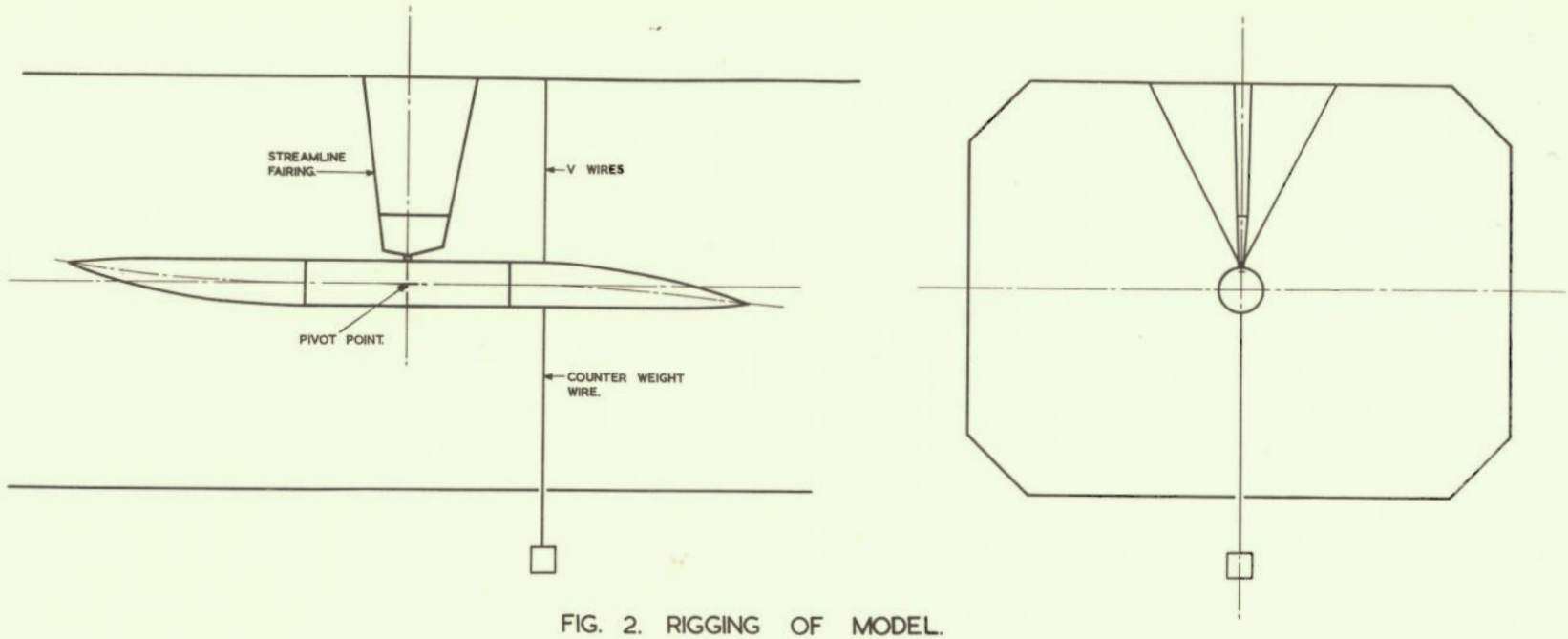

FIG. 2. RIGGING OF MODEL.

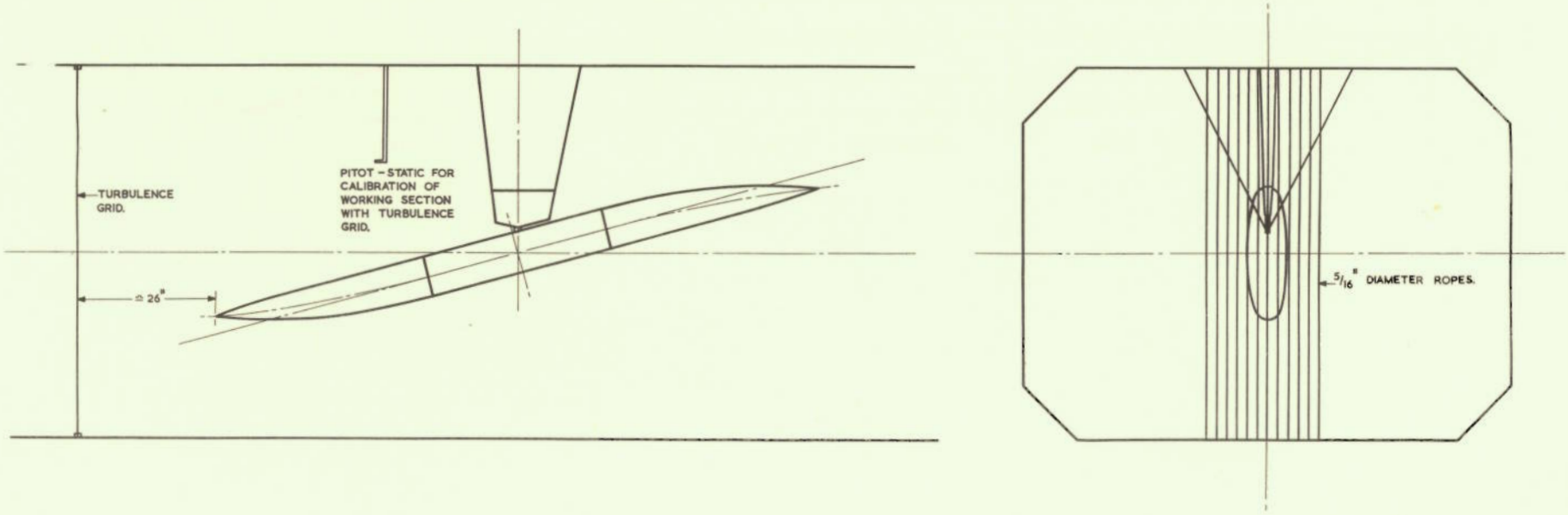

FIG. 3. TURBULENCE GRID & POSITION OF CALIBRATING PITOT-STATIC TUBE.

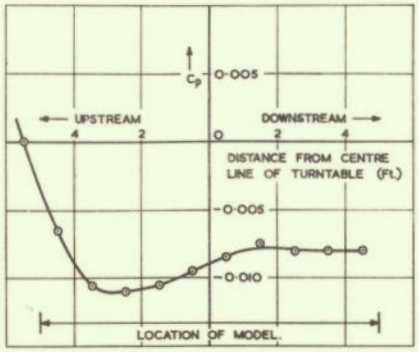

FIG. 4. STATIC PRESSURE DISTRIBUTION ALONG CENTRE LINE OF WORKING SECTION.

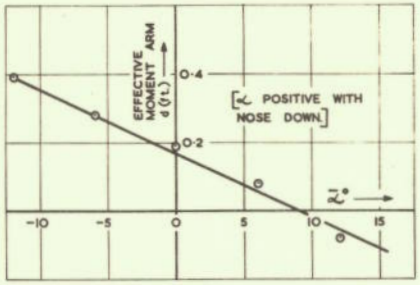

FIG. 6a.

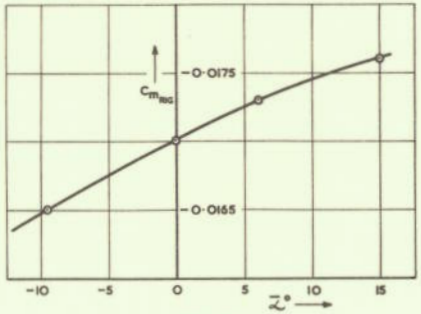

FIG. 6b.

ESTIMATED PITCHING MOMENT OF RIG TAIL WIRES.

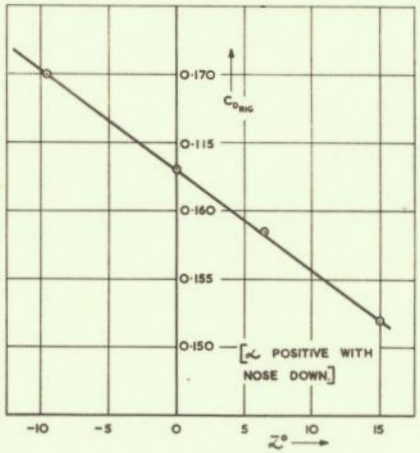

FIG. 5. ESTIMATED DRAG OF RIG TAIL WIRES.

$C_{D_{RIG}} \sim \alpha$

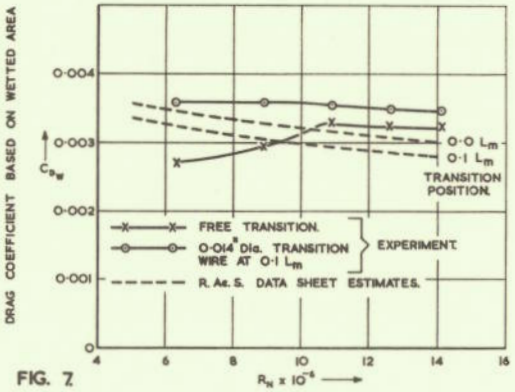

FIG. 7

VARIATION OF DRAG COEFFICIENT WITH REYNOLDS NUMBER BODY OF REVOLUTION. $\alpha = 0°$

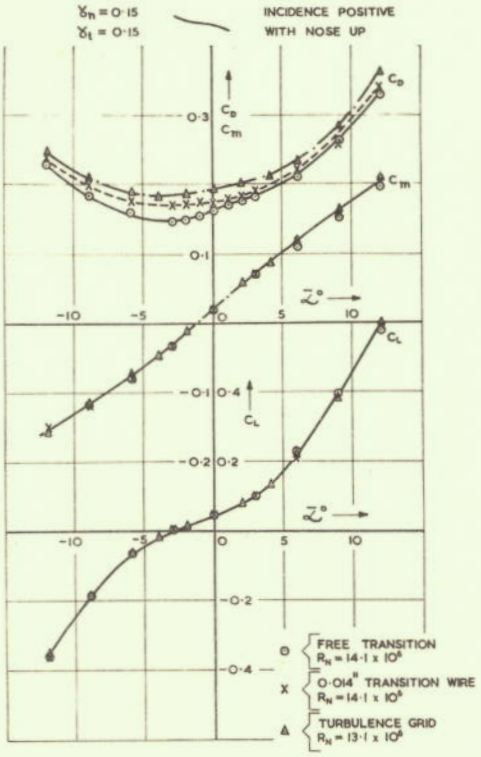

FIG. 8. EFFECT OF VARYING THE BOUNDARY LAYER.

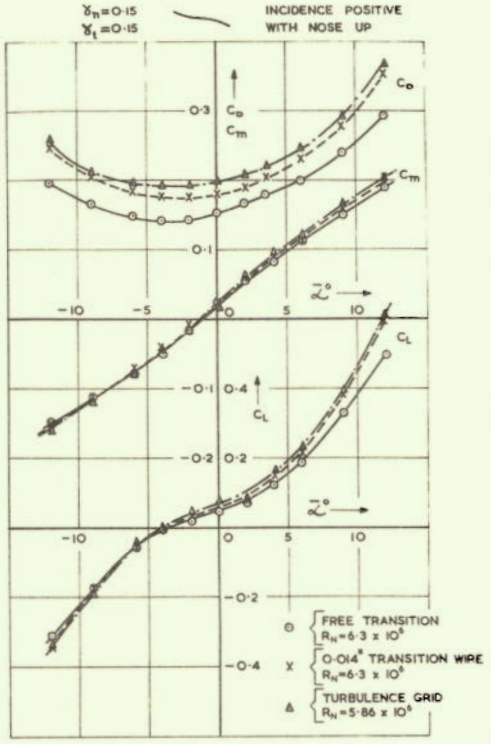

FIG. 9. EFFECT OF VARYING THE BOUNDARY LAYER.

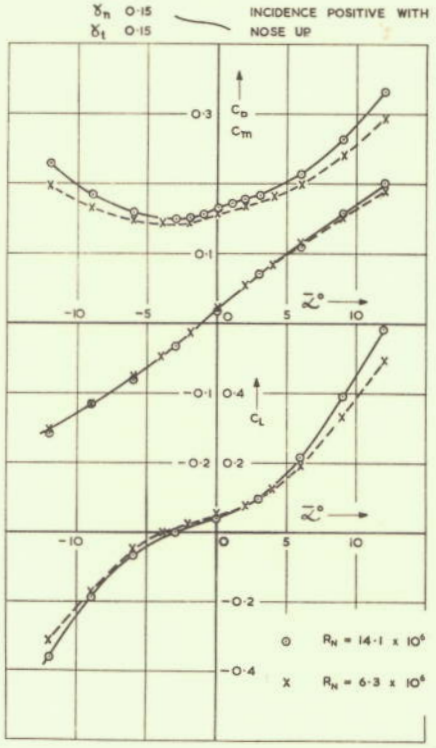

FIG. 10. EFFECT OF VARYING REYNOLDS NUMBER.
FREE TRANSITION.

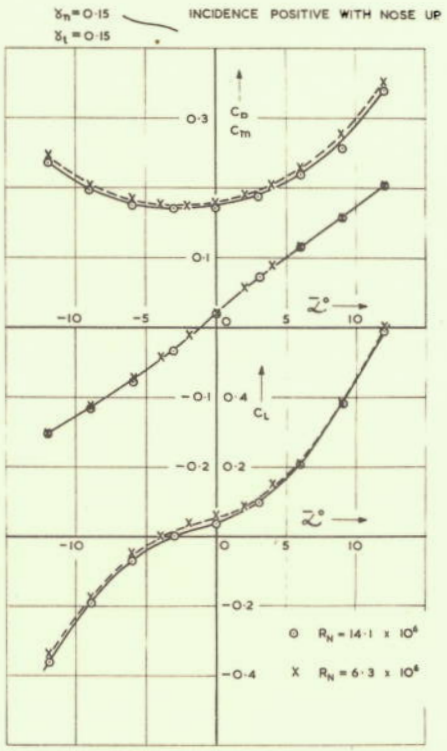

FIG. 11. EFFECT OF VARYING REYNOLDS NUMBER.
0·014" TRANSITION WIRES.

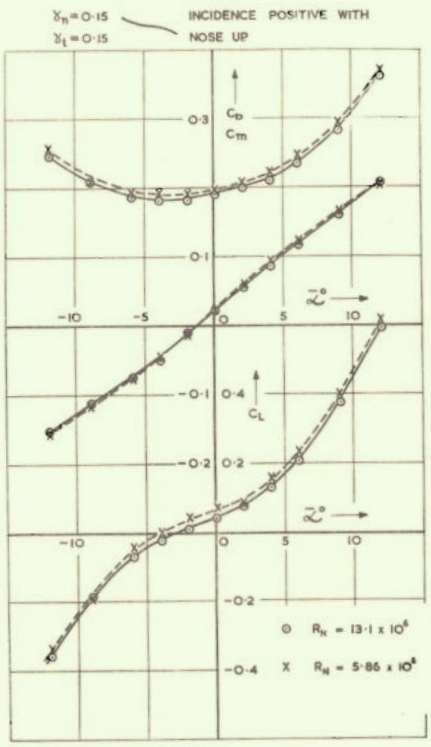

FIG. 12. EFFECT OF VARYING REYNOLDS NUMBER.
TURBULENCE GRID.

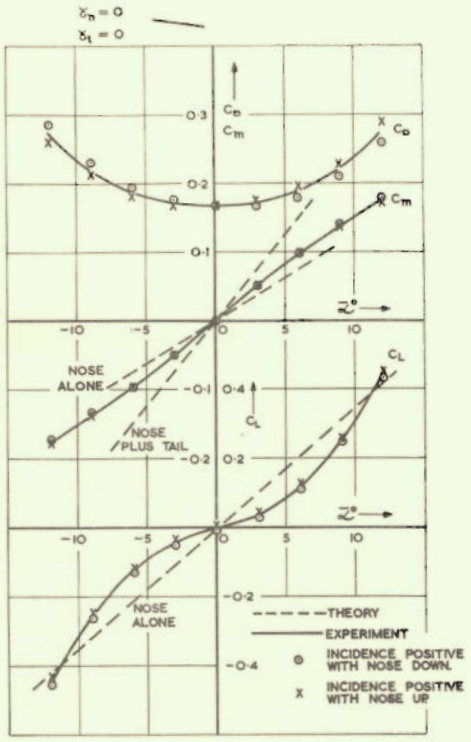

FIG. 13. BODY OF REVOLUTION.
$R_N = 14.1 \times 10^6$ 0·014" TRANSITION WIRE.

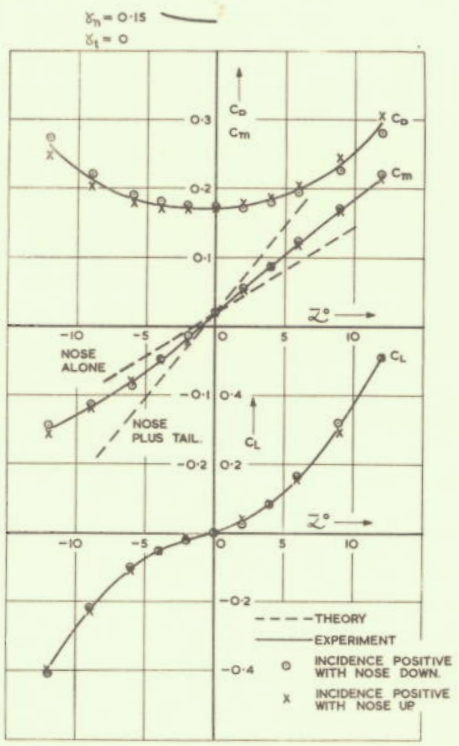

FIG. 14. NOSE CAMBER.
$R_N = 14.1 \times 10^6$ 0·014" TRANSITION WIRE.

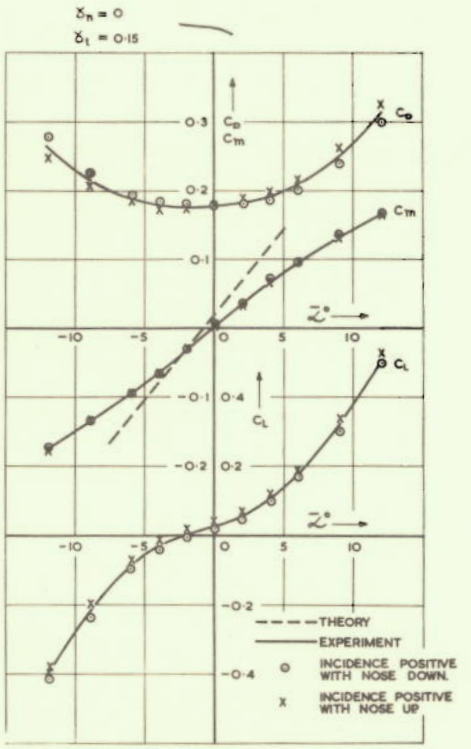

FIG. 15. TAIL CAMBER.
$R_N = 14.1 \times 10^6$ 0·014" TRANSITION WIRE.

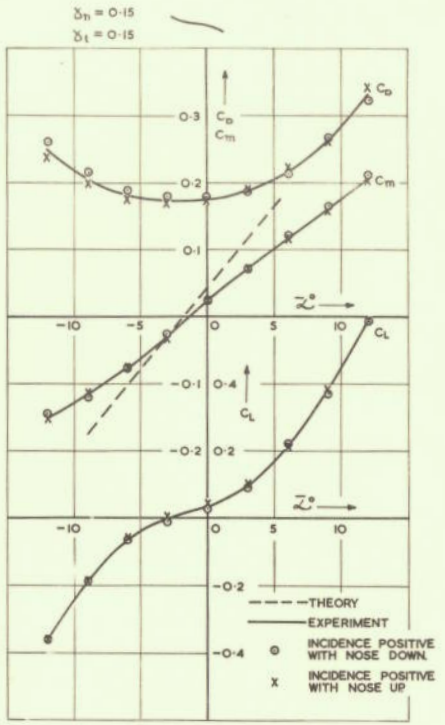

FIG. 16. NOSE AND TAIL CAMBER.
$R_N = 14{\cdot}1 \times 10^6$ 0·014" TRANSITION WIRE.

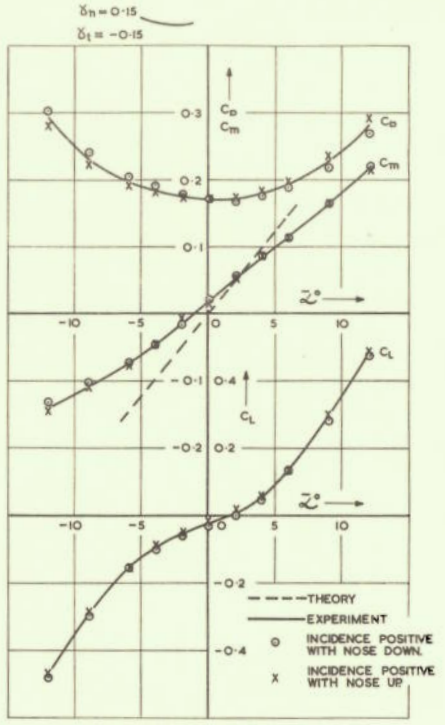

FIG. 17. NOSE AND NEGATIVE TAIL CAMBER.
$R_N = 14{\cdot}1 \times 10^6$ 0·014" TRANSITION WIRE.

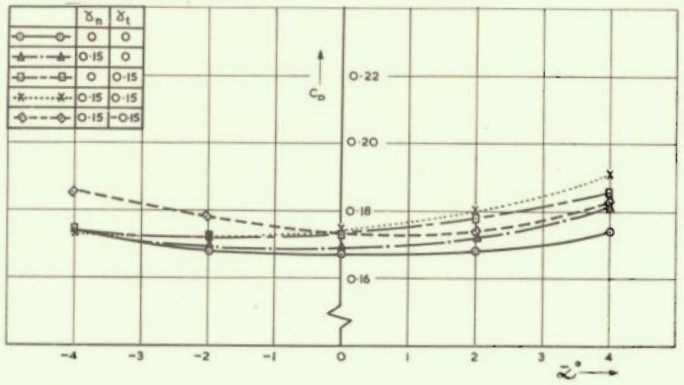

FIG. 18

$C_D \sim \alpha$

$R_N = 14{\cdot}1 \times 10^6$ 0·014" TRANSITION WIRE GLUED TO NOSE.

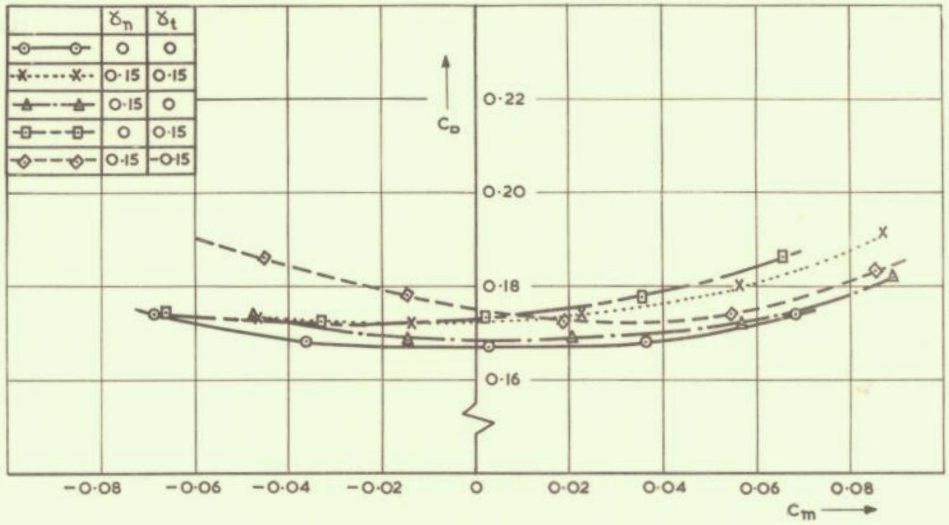

FIG. 19.

$C_D \sim C_m$

$R_N = 14{\cdot}1 \times 10^6$ 0·014" TRANSITION WIRE GLUED TO NOSE.

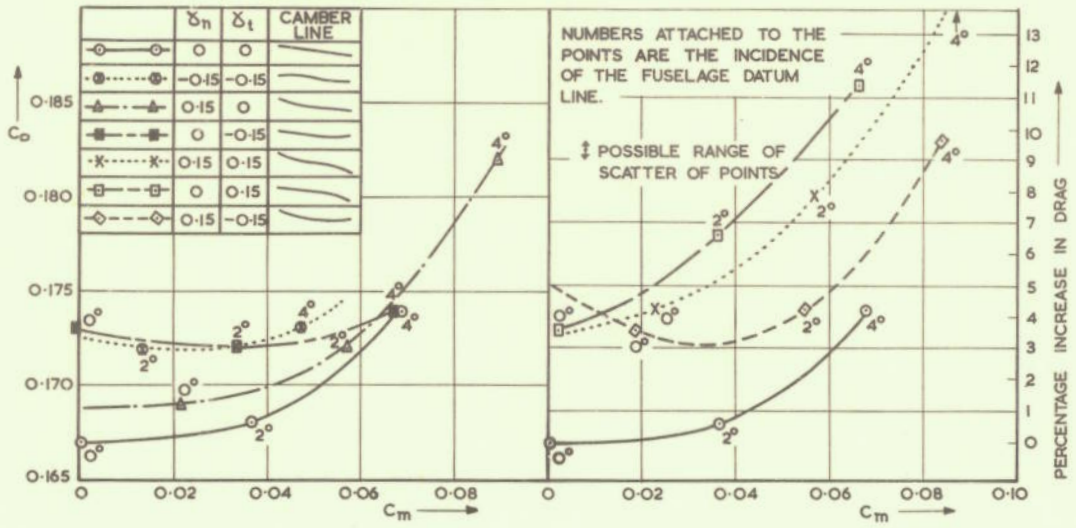

FIG. 20. COMPARISON OF THE DRAG OF VARIOUS CONFIGURATIONS.

$R_N = 14{\cdot}1 \times 10^6$ 0·014" TRANSITION WIRE GLUED TO NOSE.

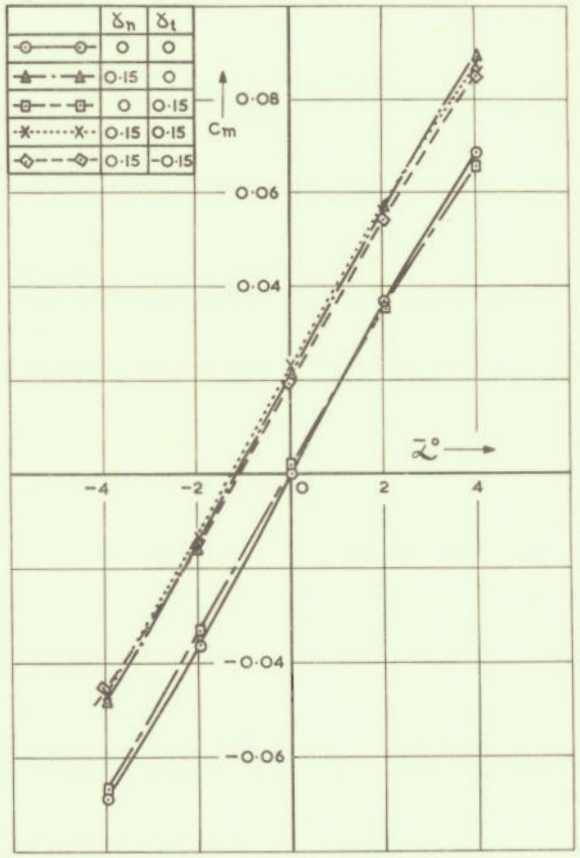

FIG. 21.

$C_m \sim \bar{\alpha}$

$R_N = 14{\cdot}1 \times 10^6$ 0·014" TRANSITION WIRE GLUED TO NOSE

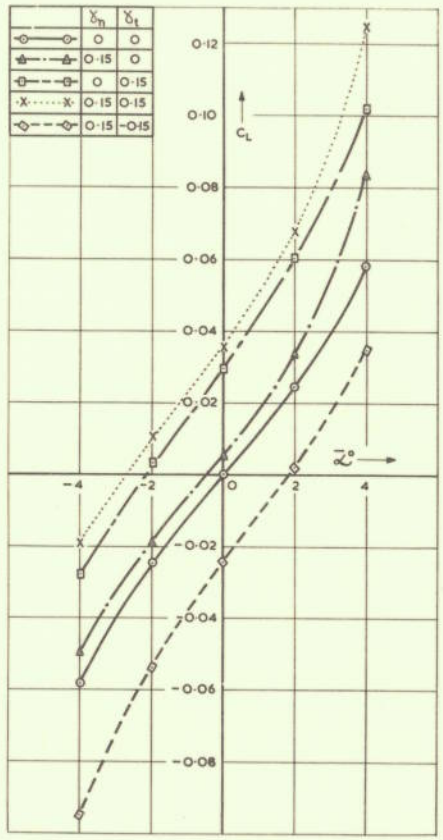

FIG. 22.

$C_L \sim \mathcal{Z}$

$R_N = 14{\cdot}1 \times 10^6$ 0·014" TRANSITION WIRE GLUED TO NOSE.

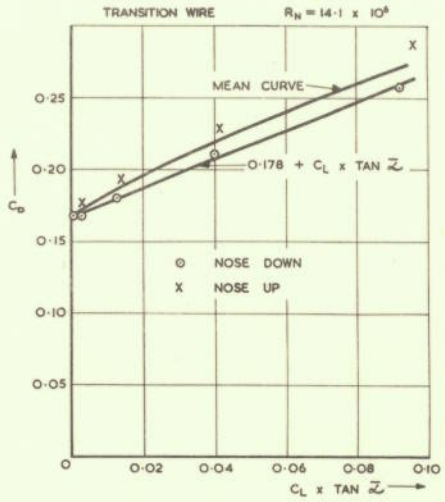

FIG. 23. BODY OF REVOLUTION.

$C_D \sim C_L \times \tan \mathcal{Z}$

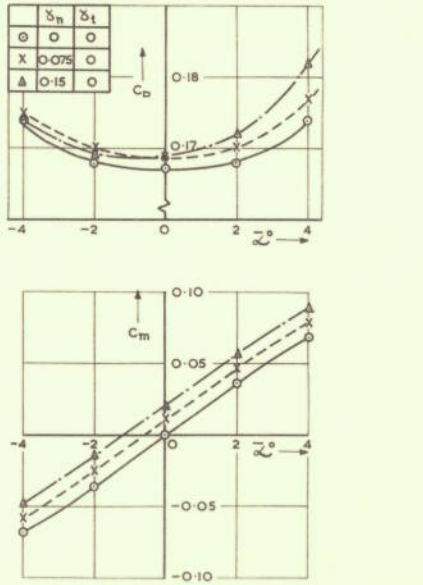

FIG. 24. EFFECT OF VARYING NOSE CAMBER

$R_N = 14{\cdot}1 \times 10^6$ 0·014" TRANSITION WIRE GLUED TO NOSE.